Molecular Dynamics Simulations of Staphylococcal Nuclease: Properties of Water at the Protein Surface

Nikolai Smolin and Roland Winter*

Department of Chemistry, Physical Chemistry I, University of Dortmund, Otto-Hahn Str. 6, D-44227 Dortmund, Germany

Received: June 4, 2004; In Final Form: July 30, 2004

We report on a molecular dynamics study of fully hydrated, native staphylococcal nuclease (SNase). Besides the global structural properties and fluctuations of the protein structure, a detailed analysis of the structural properties of the water at the protein surface (density profile, coordination numbers, hydrogen-bond distribution) was carried out. Taking into account the excluded volume effect, we found that the average density of the first hydration shell of SNase is about 0.3−0.6% larger than that of the bulk solvent. The perturbation of the water hydrogen-bonded network extends roughly two or three water layers from the protein surface at ambient temperature (300 K), and a bimodal density profile of water is observed at the protein interface. The data clearly show that the first peak of the water density profile arises from water molecules that are bonded to polar atoms (N and O) at the surface of SNase, whereas the second peak corresponds to the localization of water molecules near apolar atoms (C). A further analysis of the structural properties of water at the protein surface in terms of non-short-circuited hydrogen-bonded water rings of sizes three to nine molecules evidences the existence of clusters of water rings that are located in the first hydration shell of side chain carbon atoms and bonded to the polar side chain and/or backbone atoms by one or two hydrogen bonds. Also, we observed water rings at distances of 4−6 Å that are bonded to oxygen or nitrogen atoms of the protein by hydrogen bonds and oriented essentially perpendicular to the protein surface. Most of the large polygons have centers located at rather short distances to protein atoms, indicating that these large rings are sitting close to the surface of the protein, surrounding some of the polar amino acid side chains. The pentagon−pentagon and pentagon−hexagon radial distribution functions for the water rings near the protein surface exhibit also some type of arrangement of water molecules reminescent of the structure of clathrate-like cages.

1. Introduction

Water plays an important role for understanding the structure, dynamics, and functionality of biological macromolecules, such as proteins. A variety of structural and dynamical properties of the hydration water of proteins are reviewed and compared with those of the bulk and with corresponding experimental results in refs 1 and 2. The behavior of water at the protein surface has been the subject of a number of molecular dynamics simulations as well.[3−18] Despite of the data already available, there is still a lack of knowledge on the ordering of water molecules and the structural characteristics of the H-bond network at the protein surface.

One of the important structural features of water is the presence of an H-bond network, which can be characterized by a distribution of hydrogen-bonded polygons of water molecules.[19−23] The protein−water interface is characterized by the occurrence of H-bonds formed between the protein and surrounding water and an H-bond network of water in the interfacial region of the protein. For enzymatic activity, transfer of protons along chains of hydrogen-bonded water molecules on the surface of the protein, with long-range proton movement over H-bond networks of water in the hydrated shell, is an important issue. As for a further example of the structural organization of the solvent within the hydration shell, there is a significant increase in heat capacity when proteins are unfolded or when hydrophobic compounds are dissolved in water, and this change in heat capacity is a linear function of the area of the hydrophobic surface. The large and positive heat capacity change is generally attributed to the extra heat needed to "melt" the ordered water structure near hydrophobic groups exposed to water. In general, the structural characteristics of the H-bond network around the protein is expected to be strongly dependent on the chemical properties of the amino acids (aa) and atoms located at the protein surface.

The water structure has been shown to be very dependent on the chemical properties and the curvature of the surface near which the water molecules are located. The structure of liquid water at hydrophobic and hydrophilic surfaces has been the subject of molecular dynamics simulation,[24,25] and the results show that the hydration structure of large hydrophobic surfaces may be very different from that of small hydrophobic molecules. Recently, molecular dynamics simulation was also used for investigating the structure of water droplets on graphite.[26] Moreover, the behavior of water has been investigated by Gibbs ensemble Monte Carlo simulations in cylindrical and spherical nanopores as a function of the radius of the pores and the strength of the water−substrate interaction (from hydrocarbon-like to metal-like).[27−29] In the computer simulations it was also observed that orientation preferences for water molecules in the first hydration shell around Lennard-Jones solutes are loosely reminiscent of the structure of clathrates.[30] Zichi and Rossky[31] presented a detailed geometrical analysis of the solvent in an aqueous solution containing two nonpolar atomic solutes. The analysis revealed the clathrate-like tendency for solvating water

10.1021/jp047579y CCC: $27.50
Published on Web 09/10/2004

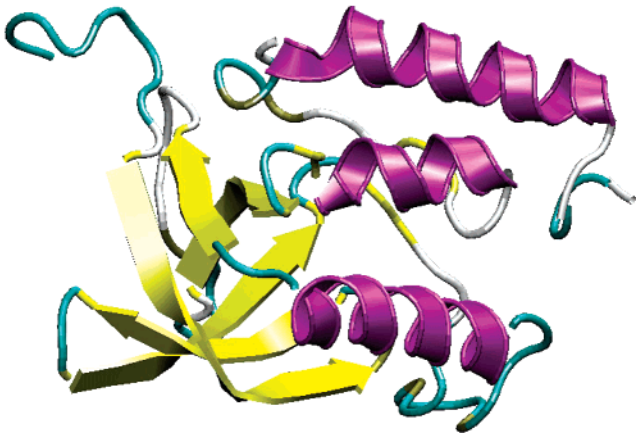

Figure 1. Schematic drawing of the native state structure of SNase taken from the coordinates of Hynes and Fox[59] (1stn.pdb). The diagram was prepared using the program VMD.[68] SNase is a small globular protein of molecular mass 16.8 kDa that contains 149 amino acid residues and no disulfide bonds. The backbone of SNase forms a five-stranded β-barrel and three α-helices.

to form convex hydrogen-bonded networks around nonpolar solutes. Hydrophobic hydration of amphipathic peptides[32] was studied in terms of the molecular orientation of water relative to the solute surfaces. These works were concerned only with the orientational distribution of water molecules in the first hydration shell. Head-Gordon[33] investigated the structural properties of water around hydrophobic groups in terms of water polygons, whose correlations can directly be compared with clathrate arrangements. Recent neutron scattering experiments[34] revealed that the changes between the structural differences of water around hydrophobic amino acids and bulk water at room temperature is analogous to the changes that are observed between ambient temperature water and supercooled water, respectively. Molecular dynamics simulation was also used for a structural analysis of the hydration shells near leucine and glutamine amino acid residues in terms of hydrogen-bonded water polygons,[35] and it was found that the hydration structure around the leucine side chain is more ordered than water near the glutamine side chain, while it is similar and less ordered near their backbones. Water rings forming clathrate-like arrangements have been found near the hydrophobic surfaces of protein[36,37] and DNA[38] as well.

The focus of our present study is to investigate in detail the structural properties of native staphylococcal nuclease (SNase), the water−protein H-bond network compared to the bulk water behavior, and the water−water H-bond network at the protein surface. SNase is a small globular protein of 149 amino acid residues that forms three α-helices and a five-stranded β-barrel (Figure 1). The protein has a large positive charge (+12 *e*) at pH 7.0 and ∼20% of the surface is covered by hydrophobic residues. Some structural, thermodynamic, and dynamic properties of native, mutated, truncated, and denaturated SNase were studied in experimental work,[39−50] in theoretical studies,[51,52] and by molecular dynamics (MD) simulations.[47,53−57] To our knowledge, no simulations have been reported on the structural properties of water at the protein surface, although a large body of experimental work on the hydration properties of the protein has been carried out, which calls for a molecular level understanding of the properties of water at its surface.[48] In particular, there is a strong need to quantify structural changes that occur in successive layers of the hydration shell, thus characterizing the range, or persistence length, of the structural changes that have long been believed to occur at the surface of aa side chains. To this end, we focus on the location of water and on the protein−water H-bond network as a function of amino acid sequence and residue type, on the structural properties of water (density, coordination number, and number of water−water H-bonds) as a function of distance from the protein atoms, on the H-bond structure of the water in terms of "non-short-circuited" rings (e.g., "clathrate-like behavior") of hydrogen-bonded water molecules, and on the correlation functions of water polygons near the protein surface in this study.

2. Methods

2.1. Molecular Dynamics Simulation of the Protein−Water System. To construct the native protein, crystallographic heavy atom coordinates were obtained from the Protein Data Bank[58] (PDB, www.pdb.org), entry 1STN.[59] Residues 1−6 and 142−149 are disordered in the crystal. The starting structure of the protein for the simulation was completed by adding coordinates for residues 1−6 (taken from PDB set 2SNS) and constructing residues 142−149 with AMBER 6.0.[60] For removing bad contacts and adopting our system to the force field, energy minimization was carried out with the steepest descent and conjugate gradient methods. Eighty-five water molecules were identified crystallographically in 1STN and were included in the starting set. The MD simulations were performed using AMBER 6.0 and the all-atom force field by Cornell et al.,[61] and the particle mesh Ewald (PME)[62] was used for the calculation of electrostatic interactions. All protein atoms were explicitly included in the simulations. The protein structure was solvated by repeated overlays of an equilibrated cubic volume of TIP3P[63] water molecules to fill a truncated octahedron box. The dimensions were chosen such that the minimum distance between the edge of the box and the protein was more than 12 Å in the starting structure. Since in the protonation state given the total charge of SNase is +12 *e*, 12 chloride counterions were added to provide a neutral simulation cell.

Equilibration was performed by placing a harmonic position restraining force constant equal to 104 kJ·mol^{-1} on all solute atoms, followed by 15 ps of constant volume MD, during which only solvent molecules were allowed to move, and the temperature was raised from 100 to 300 K during the first 4 ps. The resulting system was then equilibrated through 15 ps of NVT-MD at 300 K, in which the counterions and water molecules were restrained and the protein was able to move. The initial setup was then finished by a short, 3 ps NVT-MD run (without restrains) at 300 K to yield the initial configuration that contains the protein, 12 chloride ions, and 8604 water molecules in a truncated octahedron box. This initial configuration was used as the starting point for the simulations of the protein in pure water.

The simulation was performed at NPT conditions and at a residue-based cutoff of 10 Å for van der Waals interactions. The temperature was kept constant by a Berendsen thermostat[64] (weak coupling) with a coupling time of 0.5 ps. In the constant-pressure simulations, the pressure was kept by weak coupling to an external bath[64] with a relaxation time of 1.0 ps. The time step was 2 fs, and the bonds involving hydrogen are constrained using the SHAKE algorithm,[65] with a relative tolerance of 10^{-5}. The simulation at 300 K and 1 bar was continued for 7.2 ns. For analysis purposes, the trajectory from 5.2 to 7.2 ns was used, and coordinates were saved every 0.2 ps.

The trajectories were analyzed using the AMBER analysis modules PTRAJ and CARNAL for the calculation of the root-mean-square deviations (rmsd), the root-mean-square fluctua-

tions (rmsf), and the radius of gyration (R_g). The program DSSP[66] was used for the calculation of the solvent accessible surface area (SASA) and the determination of the secondary structure. The volume of the protein was calculated with the program Mol_Volume.[67] A 1.4-Å radius for the probe sphere was used for all calculations of volume and SASA. All snapshots were prepared using the program VMD.[68]

2.2. Analysis of the H-Bond Network. We have analyzed the protein−water and water−water hydrogen bonds in great detail. For the analysis of hydrogen bonds, the following geometric criterion was used: The proton-donor to heavy-atom acceptor distance must be less than 2.5 Å, and the hydrogen-bond angle must be greater than 120°. To detect "non-short-circuited" rings of hydrogen-bonded water molecules, we used the definition of Rahman and Stillinger.[19] These are polygons with three or more sides and no pairs whose vertexes are linked by a hydrogen-bond path shorter (in number of bonds, not geometrical length) than the minimal path within the polygon itself. The ring position is defined as the center of mass of the assembly of water molecules forming the polygon. Polygon counts are enumerated as follows: For every water molecule we determine all H-bond connections; if a given water molecule has fewer than two H-bonds with the other water molecules, it can never serve as a polygon vortex. First, we determined all triangles, i.e., H-bonded chains that are closed in three steps. All these triangles were counted because any three molecules mutually bonded to form a triangle cannot be short-circuited. Next, we searched for all tetragons, i.e., polygons that are closed in four steps and non-short-circuited (no H-bonds between opposite vertexes). This procedure continues for successively larger polygons. In the pentagons' case, we checked that any three or four water molecules in a given pentagon are not involved in triangles or tetragons, respectively. Similarly, regarding hexagons, additionally, we made sure that any five water molecules are not involved in pentagons. We terminated this counting of the polygons at nonagons (nine-sided polygons). For example, for typical ices (hexagonal and cubic), the size of the polygons of the hydrogen-bonded water molecules is six; in some others ices, polygons with sizes from four to eight were found.[69] For clathrate-like structures to be evident, the distribution along the hydrophobic surface is expected to be dominated by pentagons, with significant depletion of hexagons and larger polygons.

3. Results

3.1. Structural Properties of SNase and Fluctuations of Its Secondary Structure. The rmsd of the backbone atoms from the crystallographic structure, the R_g, the SASA, and the volume were monitored as a function of time (Figure 2) up to a simulation time of 7.2 ns. The rmsd of the complete backbone from the crystal structure stabilized after ~1.5 ns at its final average value of 2.2 (±0.3) Å. As expected, the main deviations are localized in the N-terminal region. Omitting this region from the calculation results in a rmsd value for the heavy backbone atoms of 1.6 (±0.1) Å. The radius of gyration stabilized at 15.70 (±0.1) Å, which is 2% larger than the R_g-value of SNase in the crystal structure.[59] The solvent accessible surface area is 9417 (±160) Å^2, according to a 7% increase compared to the X-ray crystal structure.[59] The SASA may be divided between residues into 19.86 (±0.6)% nonpolar, 24.12 (±0.6)% polar neutral, 40.27 (±0.8)% positively charged, and 15.75 (±0.5)% negatively charged amino acid residues, respectively (Table 1). The volume of the protein increases from the start value of 33 400 to 33 650 Å^3.

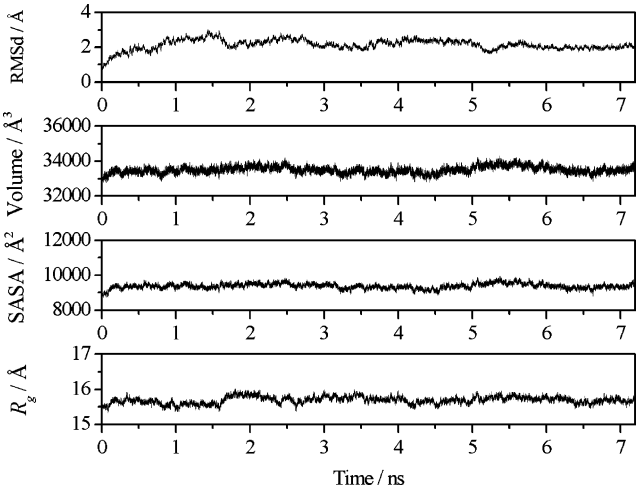

Figure 2. Time evolution of global structural properties of SNase from MD simulation: radius of gyration (R_g); the root-mean-square deviations (rmsd) from the starting structure, which was computed over all protein backbone atoms; the solvent accessible surface area (SASA); and volume of the protein.

TABLE 1: Solvent Accessible Surface Area (SASA) and Average Fractional Solvent Accessibility (f_{sa}) for All Residues and for the Various Types of Amino Acid (aa) Residues of Fully Hydrated SNase[a]

types of residues	no. of aa residues	% in aa sequence	SASA (Å^2)	% of SASA	f_{sa}
all residues	149	100	9417(160)	100	0.218
nonpolar	62	41.61	1871(60)	19.86(0.6)	0.125
polar, neutral	33	22.15	2271(70)	24.12(0.6)	0.233
positively charged	33	22.15	3792(74)	40.27(0.6)	0.365
negatively charged	21	14.09	1483(50)	15.75(0.6)	0.238

[a] Standard deviations are given in parentheses.

The time evaluation of secondary structure and the root-mean-square fluctuations of all protein backbone atoms are given in Figure 3. For calculating rmsf, we used the last two nanoseconds of the simulation only. We find that α-helices make up 23.6 (±1.3)% and β-strands 25.5 (±1.2)% of all secondary structure of SNase, in very good agreement with the X-ray crystal structure data (22.1% α-helices, 26.2% β-strands).[59] The rest are turns, loops, and random, nonordered structures and other helices. As expected, the most stable parts of the secondary structure of the protein are the three α-helices and the five β-strands. Fluctuating parts of the protein are turns and bends between the α-helices and β-strands as well as the N-terminal region (Figure 3).

To explore to what degree each residue within the amino acid sequence is exposed to the solvent, we calculated their time-averaged fractional solvent accessibilities[70] as $f_{sa} = A_{protein}/A_{free}$, where $A_{protein}$ is the solvent accessible surface area of a particular residue in the presence of the other surrounding residues of SNase, while A_{free} is the corresponding surface area if no other aa residues are present, i.e., of the free residue. Figure 4a shows the fractional solvent accessibilities of all residues along the amino acid sequence of SNase. Typically, f_{sa} values vary from 0 to ~0.5. We find that the average fractional solvent accessibilities for positively and negatively charged amino acids are 0.365 and 0.238, respectively, while the f_{sa} value for neutral polar and nonpolar groups are 0.233 and 0.125, respectively (Table 1). As expected, the nonpolar groups make up the smallest population of water exposed residues.

3.2. Water−Protein Interactions. Since we want to focus on the structural properties of the water molecules that interact with the protein surface, we first removed two strongly bound

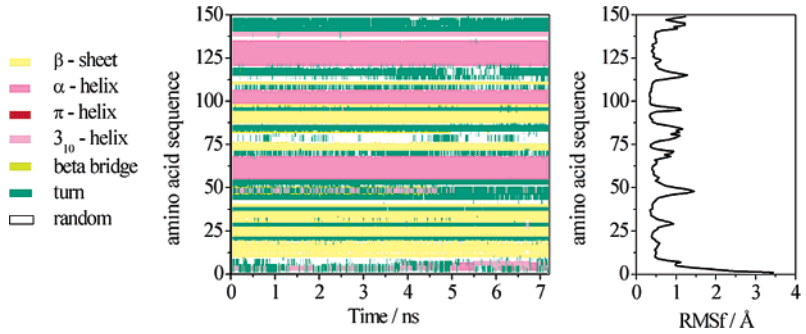

Figure 3. (left) Secondary structure of SNase as a function of simulation time (DSSP classification[66]). (right) Root-mean-square fluctuations (rmsf) of the protein backbone atoms calculated over the last 2 ns of the simulation as a function of residue sequence number.

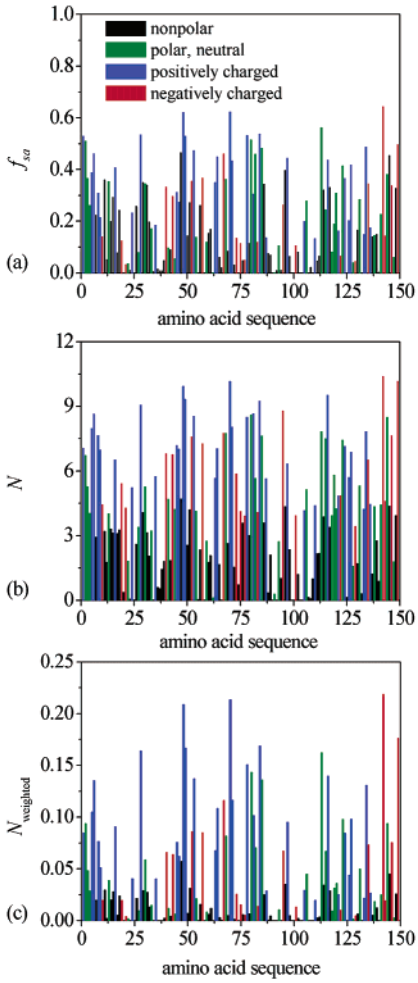

Figure 4. (a) Fractional solvent accessibilities (f_{sa}) as a function of residue sequence number and type of aa residue. (b) The average coordination number of residues (number of water molecules closer than 3.5 Å to any heavy atom of the amino acids) along the aa sequence of SNase. (c) The SASA-weighted average coordination number of residues (the average coordination number multiplied by the ratio of the SASA of a given aa residue to the SASA of the whole protein) along the aa sequence of SNase.

internal water molecules from our analysis: one water molecule bridging two aa (Val104 and Trp140) and a second water molecule residing in an internal pocket. For determining the hydrational properties of each aa residue, we first calculated the average coordination number, *N*, of each residue of SNase (Figure 4b). The coordination number calculated corresponds to the number of water molecules of closest approach, i.e., that are located within a shell of 3.5 Å around any heavy atom (carbon, nitrogen, oxygen, and sulfur) of the particular aa

TABLE 2: Time-Average of the Water Coordination Number of the Various Types of Amino Acid Residues of Fully Hydrated SNase as Well as the Corresponding Values of Their Backbone/Side Chain Atoms[a]

	coordination number				
		backbone		side chain	
type of residues	total	polar atoms	apolar atoms	polar atoms	apolar atoms
nonpolar	102.2(5.5)	79.4(4.2)	24.8(2.1)	2.0(0.8)	39.1(3.6)
polar, neutral	146.0(7.4)	48.8(3.3)	11.2(2.3)	95.0(6.3)	49.5(4.1)
positively charged	220.7(9.2)	58.1(3.8)	17.2(2.2)	137.3(7.5)	108.9(6.7)
negatively charged	125.2(6.5)	35.1(2.9)	12.0(1.9)	110.7(5.5)	69.5(4.2)

[a] Standard deviations are given in parentheses.

residue. Figure 4b shows that the level of hydration is particularly high around polar/charged residues. Only few nonpolar residues have more than one water in their first hydration shell and probably only because of neighboring polar residues; their maximum coordination numbers may reach ~4. Most of the hydrating water molecules thus arrange near positively and negatively charged aa residues. In Table 2, the time-averaged coordination numbers for the backbone and side chain atoms are summarized. As the side-chain atoms of the polar aa residues are more exposed to the solvent, their average water coordination numbers are highest. The average number of water molecules within a shell of 3.5 Å around the whole protein is 455 (±12). When we compare parts a and b of Figure 4, we note that the fractional solvent accessibility for some residues with relatively high values of *N* is very small or even close to zero, and the hydration level of the different aa residues depends significantly on the local solvent accessible surface area. To provide a more reliable comparison of the hydration level of the different types of aa residues, we calculated an SASA-weighted average coordination number, $N_{weighted}$, for each residue along the aa sequence of the protein (Figure 4c) by multiplication of *N* with the ratio of the SASA of a given aa residue to the SASA of the whole protein. Hence, high values of $N_{weighted}$ in fact reveal large levels of hydration, while low values correspond to cases when the SASA of an aa residue is small or even close to zero. If the average coordination number is relatively high and the residual SASA very small or even close to zero due to the local protein topography, as often in the case of nonpolar aa residues, all hydration water may be hydrogen bonded to neighboring water exposed to (mostly polar) residues. Comparison of Figures 4c, 5a, and 5c exhibits that, for polar aa residues, decreasing values of $N_{weighted}$ with respect to *N* are due to the fact that only polar atoms are accessible to the water molecules, since they are able to form strong H-bonds.

Parts a and c of Figure 5 display the average number of protein−water hydrogen bonds for each residue as a function of the amino acid sequence and residue type for the situation

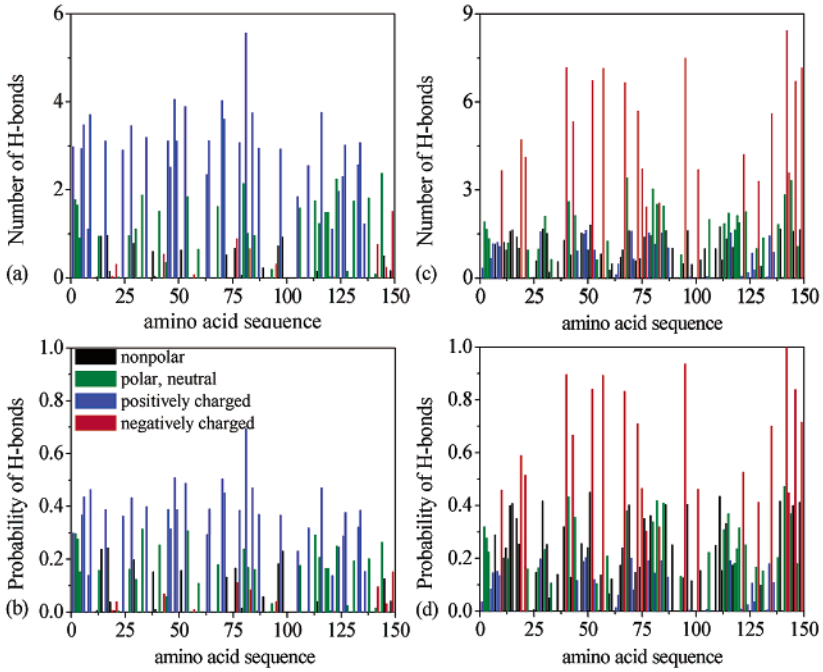

Figure 5. The average number of protein−water hydrogen bonds (a) when the protein atoms serve as a donor and (c) when the protein atoms act as a acceptor, as a function of residue sequence number. (b) The average probability of protein−water hydrogen bonds (the number of H-bonds divided by the number of possible H-bonds) (b) when the protein atoms serve as a donor and (d) when the protein atoms act as an acceptor, as a function of aa residue sequence number.

TABLE 3: Time-Averaged Number of Protein−Water Hydrogen Bonds of Various Types of Amino Acid Residues of Fully Hydrated SNase as Well as the Corresponding Values of Their Backbone/Side Chain Atoms[a]

	no. of H-bonds					
	total		backbone		side chain	
type of residues	donor H-bond	acceptor H-bond	donor H-bond	acceptor H-bond	donor H-bond	acceptor H-bond
nonpolar	9.2(1.1)	46.8(2.3)	8.2(0.8)	46.4(2.2)	1.0(0.4)	0.4(0.3)
polar, neutral	35.6(2.1)	55.0(4.5)	9.1(1.5)	22.3(2.2)	26.5(2.5)	32.7(2.8)
positively charged	98.5(4.3)	24.6(2.2)	13.6(2.1)	24.6(2.1)	84.9(3.7)	0.0
negatively charged	5.4(1.3)	110.0(7.4)	4.1(0.8)	20.8(2.2)	1.3(0.4)	89.2(6.5)

[a] Standard deviations are given in parentheses.

when hydrogen atoms from the protein act as donor (donor H-bond) and when polar atoms of the protein act as acceptor (acceptor H-bond) of hydrogen bonds, respectively. The time-averaged number of donor H-bonds and acceptor H-bonds of our protein amounts to 149 (±6) and 230 (±7), respectively. It can be clearly seen (Table 3) that the largest numbers of H-bonds essentially occur at the side chains of the negatively charged (Asp, Glu, and C-terminal) and positively charged (Lys, Arg, His, and N-terminal) aa residues, which is due to the fact that they are largely exposed to the solvent. Average numbers of hydrogen bonds for polar and negatively and positively charged aa residues are 2.75, 5.50, and 3.73. Maximal numbers of protein−water hydrogen bonds for negatively charged and positively charged aa residues reach values of ∼7 and ∼4, respectively. To determine the relative propensity of an aa residue to form hydrogen bonds with water, we also calculated the average probability (the number of donor or acceptor H-bonds divided by the maximal possible number of donor or acceptor H-bonds, respectively) of protein−water hydrogen bonds (Figure 5b,d). Clearly, the probability of forming hydrogen bonds for negatively and positively charged aa residues of the protein is highest (since these residues are exposed to water), whereas that of the other types of aa residues seldom exceeds 50%, while they serve to keep the protein secondary structures (α-helices and β-strands).

3.3. Water-Density Distribution at the Protein Surface. To investigate the influence of the protein surface on the structure of water, we calculated the density profile of water, the water−water hydrogen-bond distribution, and coordination number of water as a function of distance from the protein atoms. For precise evaluation of the water-density distribution, we first calculated the volume of shells with thickness 0.1 Å as a function of the distance from the nearest heavy atoms (N, O, C, and S) of the protein, and these data were determined for every 10th saved set of coordinates of the simulation run. Figure 6 displays some of such profiles obtained from different sets of coordinates during the simulation run. The shape of the curves reflects the existence of cavities and clefts at the protein surface. For calculation of the water density profile, we counted the number of water molecules (the position of the water molecule is defined as the center of the oxygen atom) within the same shell and divided this number by the corresponding volume of their shell. Two pronounced density maxima close to the protein can be identified, at distances of 2.85 and 3.65 Å with peak heights of 0.0713 and 0.0426 $Å^{-3}$, respectively (Figure 7a). These results are in qualitative agreement with previous molecular dynamics simulations of protein solutions;[18,71] however, probably owing to the short step size (0.1 Å) used here for the calculation of the water density profile close to the

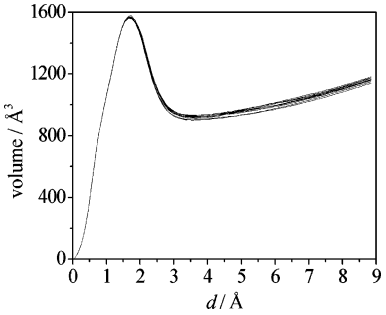

Figure 6. Volume of shells (volume of shells of space) as a function of distance from nearest protein heavy atoms. The figure shows profiles obtained from the coordinates at different stages of the simulation run.

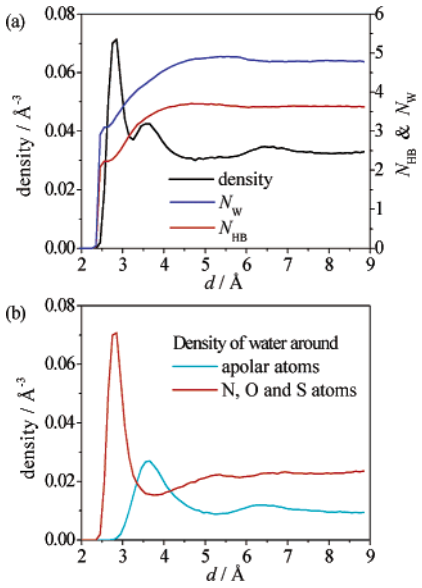

Figure 7. (a) Density profile of water (full black line), average number of water−water hydrogen bonds per water molecule (N_{HB}), and average coordination number of water molecules (N_w) as a function of distance (d) from nearest protein heavy atoms. (b) Density profile for water as a function of distance from different types of nearest protein atoms.

protein surface, we observe two distinct peaks in the density profile.

For further evaluation of the water density profile around different types of residues, we labeled the water molecules in the following way: If the nearest atom of the protein to a given water molecule is a polar atom (N, O, or S), we call this a class I water molecule; if it is a carbon atom, it is denoted a class II water molecule. The average density profiles of class I and II water molecules are depicted in Figure 7b. The number density of water at distances >7.5 Å equals the number density of bulk TIP3P water under ambient conditions (0.0329 $Å^{-3}$). These data show that, concerning structural properties, about two or three water layers are perturbed by the protein surface, only. For estimation of the average density of the first hydration shell of SNase, we calculated the number of water molecules within a shell of 4.5 Å (position of the second minimum of the density profiles of water) from any heavy atoms of the protein. The volume accessible to these water molecules is defined by the difference between the volume within a shell of 4.5 Å from the centers of any heavy atom and the corresponding solvent-excluded volume[72] (the van der Waals volume of the protein plus the interstitial volume). We obtain a 0.3% density increase over the bulk in a shell of 4.5 Å and of 0.6% in a shell of 4.0 Å. Furthermore, the data clearly show that the first peak of the water density profile arises from water molecules that are bonded to polar atoms (N, O, and S) at the surface of SNase, whereas the second peak clearly corresponds to the localization of water molecules near apolar atoms (C) (Figure 7b).

3.4. Water−Water H-Bonds near the Protein Surface. The average number of water−water H-bonds per water molecule (N_{HB}) and the average coordination number of water (N_w) as a function of distance from nearest heavy atoms of the protein are also shown in Figure 7a. In the water bulk region, an average number of hydrogen bonds of 3.64 per water molecule and an average coordination number of 4.80 are found. Both values are similar to the values found in a control MD simulation of bulk TIP3P water. The N_{HB} and N_w decrease with decreasing distance from protein atoms, which is due to consecutive substitution of water molecules by surface protein atoms. We note that these profiles exhibit a broad maximum in the region of the second minimum of the water density profile (Figure 6a). Interestingly, a similar behavior of H-bond profiles has been observed by Werder et al.[26] in their MD simulation of a water droplet on graphite. At this maximum, the average water−water H-bond number per water molecule is 3.71 (1.9% above the bulk value), and the average water coordination number of water is 4.91 (2.3% above the bulk value). We also calculated the same profiles separately for class I and II water molecules and found a similar behavior for both cases (data not shown).

3.5. Water Polygons at the Protein Interface. The density profiles of water polygons as defined in paragraph 2.2 of the Methods section are given in Figure 8a. The distributions of pentagons, hexagons, and heptagons exhibit a maximum, which is located in the region of the second minimum of the water density profile (at 4−6 Å). Interestingly, a similar behavior for pentagons and hexagons was observed by Brovchenko et al.[28] in Gibbs ensemble simulations of water in spherical pores with slightly hydrophilic surfaces. In that paper, the authors suggested from a simple geometrical analysis that such a maximum simply reflects water rings that include water molecules from the second water layer. For small water rings (3- and 4-rings), this maximum is shifted closer to the protein surface (4−4.5 Å). For 8- and 9-sided polygons, the peak height decreases, and the peak broadens and is shifted toward larger distances (∼6 Å). On the surface of the protein, polar, charged, and apolar atoms and residues are located. Hence, an analysis of the distribution of non-short-circuited hydrogen-bonded water rings was done in a way similar to that presented above for the water density profiles (Figure 8a), labeling the polygons according to the chemical nature of the protein heavy atom closest to the center of the rings. If the center of the ring is close to a carbon atom of the protein, we name that ring a class II ring; otherwise, it is a class I ring.

The plot of the number density of class II rings of sizes 4−7 exhibits a prepeak around 3−4 Å (Figure 8a, dotted lines). For a better understanding of the nature of this prepeak, we calculated the population of the class II rings as a function of distance from nearest protein heavy atoms (Figure 8b) by dividing the number of class II rings by the total number of rings in the corresponding shell at a given distance from the protein atoms. We note that a more or less pronounced first peak appears at a distance of ∼3.45 Å for all polygons, except for 3-rings, which still exhibit a shoulder in the distribution function at that distance, however. This peak corresponds to the prepeak in the density profile of class II rings (Figure 8a). The second peak shifts to larger distances with increasing ring size; it appears at 4.75 Å for 3-rings and at 6.05 Å for 7-rings. For 8- and 9-rings, a broad distribution is observed only. The first pronounced peak corresponds to class II rings with centers

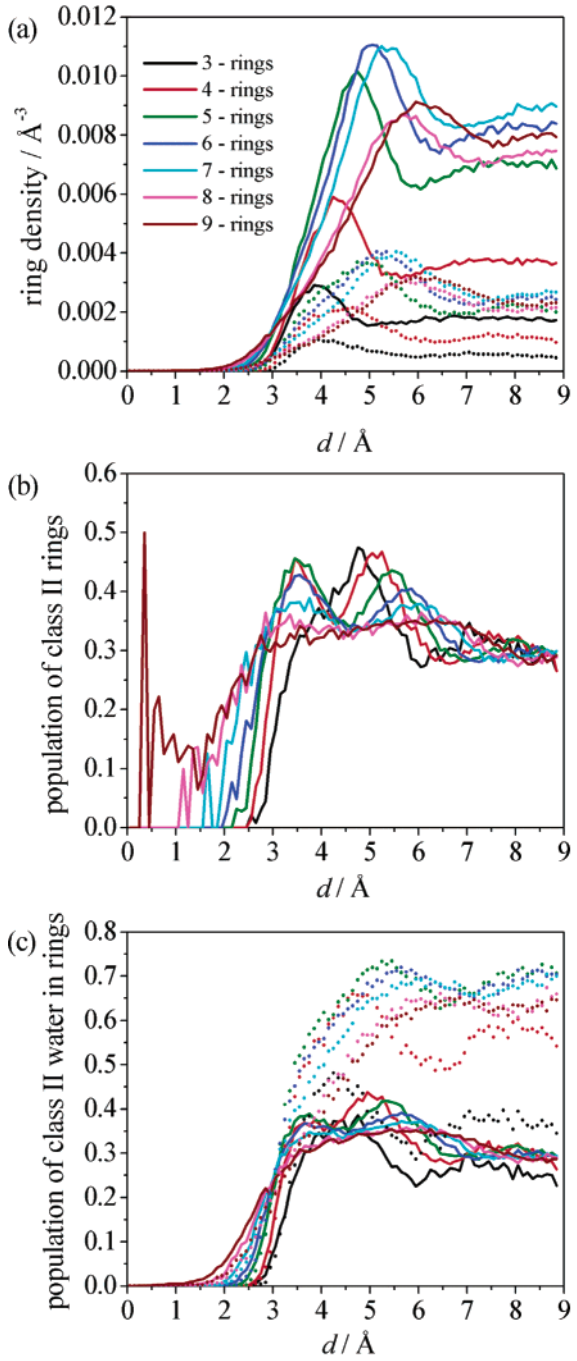

Figure 8. (a) Total number density of "non-short-circuited" water rings (solid lines) and number density of class II water rings (dotted lines) as a function of distance from nearest protein heavy atoms (class II water rings are denoted as those water rings whose center of mass is closer to a carbon atoms than to a polar atom of the protein). (b) Population of class II water rings as a function of distance from nearest protein heavy atoms. (c) The average population of class II water molecules in all water rings (solid lines) and in class II water rings (dotted lines) (class II water molecule denotes water being located closer to a carbon atom than to a polar atom of the protein).

of mass located in the first hydration shell of carbon atoms (these types of rings, evidently, are hydrogen bonded to polar side chain and/or backbone atoms), while the second peak relates to cases where some water molecules in rings are shifted to the second hydration shell of the carbon atoms. The minimum observed around 4.5 Å between the two density maxima of class II rings is due to the fact that at this location most of the water rings are class I rings and arranged in such a way that they are bonded to oxygen or nitrogen atoms of the protein by one or more hydrogen bonds, and most of their water molecules are located in the second hydration shell of the polar atoms with orientations of these rings being more perpendicular to the protein surface; the population of class II rings at this distance is lower. Interestingly, Figure 8b also reveals that a significant population (~80%) of larger polygons have centers located at rather short distances to protein atoms, indicating that these large class I rings are sitting close to the surface of the protein, surrounding some of the polar aa side chains (but the concentration of such clusters is very low, as seen in Figure 8a).

Figure 8c depicts the average population of class II water molecules in the total number of water polygons (solid lines) and in class II rings (dotted lines) as a function of distance from the protein nearest atoms. The maxima observed for the average population of class II water molecules in water polygons seem to be related to the maxima in the profiles for the population of class II rings (Figure 8b). An average population of class II water molecules at the position of the first peak in Figure 7b with values higher than 0.50 indicates that most class II rings are directly hydrogen bonded to polar protein atoms. The population of class II water in class II rings in the region of the second maximum is still higher and equals 0.65 for 4-rings and to ~0.70 for 5−7-rings, i.e., most water molecules in the class II rings are located above carbon atoms here and only very few in the second hydration shell are close to nitrogen or oxygen atoms at the protein surface. In the case of 3-rings, most of them are oriented such that only one water molecule in these rings is located above a carbon atom.

We also analyzed the distribution of water rings around different types of aa residues near the protein surface in great detail. A water ring was attributed to a particular type of aa residue if its center has the closed approach to that particular residue. The population of water rings near different types of aa residues at distances far from the protein surface (> 6.5 Å) does not change anymore and simply reflects the SASA of that particular type of residue. Upon approaching the protein surface, however, this population changes owing to local topographic properties, density changes, and specific interactions with the various aa residues. In particular, with approaching the protein surface, the fraction of rings near nonpolar and positively charged aa residues decreases while that near polar neutral and negatively charged aa residue increases. We suspect that since essentially polar atoms of the negatively charged aa are accessible to the solvent (see above) and near such groups the density is higher, the possibility of forming water rings increases. In support of that we found that in the region between 3.0 and 5.0 Å from the atoms of positively charged aa, about half of the ring atoms are located near side chain polar atoms and the other half of the ring covers the nonpolar side chain atoms. On the contrary, around negatively charged aa residues, water rings cover essentially the polar side chain atoms. This may be due to a simple size effect of the negatively charged residues having shorter side chains compared to the positively charged ones.

Parts a and b of Figure 9 display the pentagon−pentagon radial distribution function, $g_{55}(r)$, and the pentagon−hexagon cross-correlation function, $g_{56}(r)$, for the control bulk water simulation and for the protein−water interfacial region (only polygons within a shell of radius 6.5 Å around protein atoms were considered). Owing to the excluded volume effect of the protein, we normalized these correlation functions to the calculated density of the water rings in the volume between 2.0 and 6.5 Å from the centers of the protein heavy atoms.

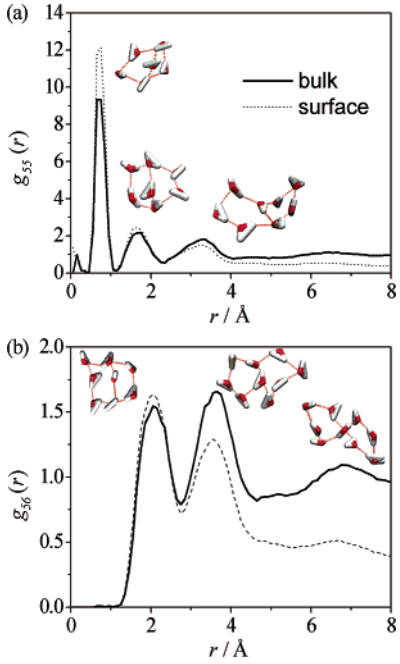

Figure 9. (a) The pentagon−pentagon and (b) the pentagon−hexagon radial distribution functions for bulk water (solid lines) and for water rings within 6.5 Å from protein heavy atoms (dashed lines). The figures visualize the arrangement of water rings corresponding to the positions of the respective correlation function.

In Figure 9a, the pentagon−pentagon radial distribution function $g_{55}(r)$ is shown. Three pronounced maxima appear, which are located at 0.75, 1.65, and 3.2 Å. The first and second peaks correspond to compact arrangements of pentagons (two or three common sites), while the peak at 3.2 Å corresponds to a more open, clathrate-like arrangement[21,23] when pentagons share only one site. Two further broad peaks appear at 4.7 Å and between 6 and 7 Å, respectively. In ref 21 the corresponding configurations are given.

Figure 9b shows the existence of three peaks for the pentagon−hexagon radial distribution function $g_{56}(r)$. Maxima of $g_{56}(r)$ at 2 and 3.6 Å correspond to cases where the pentagon and hexagon share two sites or only one site, respectively. The broad peak at 6.7 Å corresponds to configurations with common water molecules in hexagon−pentagon arrangements. Some representative arrangements are depicted at the corresponding peak positions of Figure 9b.

Despite the excluded volume effect, both correlation functions for the protein−water system exhibit distinct maxima that have a similar position and shape as the bulk water system. Some of their maxima seem to be even slightly higher. Due to the existence of distinct correlations between pentagon−pentagon and pentagon−hexagon units and the fact that the number density of water rings is rather high at distances 4−5 Å, we may infer that a significant part of these water rings are oriented essentially parallel to the protein surface.

4. Discussion

In this study we carried out a 7 ns constant pressure, constant temperature MD simulation of fully hydrated SNase. The trajectories were analyzed with respect to changes in protein global structural properties: rmsd, rmsf, SASA, volume, R_g, and secondary structure elements. The data for the rmsd and rmsf are in good agreement with previous molecular dynamics simulation of native, liganded, and unliganded SNase.[56,57] The radius of gyration is very close to the experimental value (15.7 Å),[46] and the structure of the protein is stable under the simulation conditions. Most of the SASA is covered by polar aa residues (in particular neutral and positively charged groups). The fractional solvent accessibilities for these residues are higher than those for nonpolar amino acid residues. Mainly those water molecules located in the first hydration shell of SNase around exposed side chain atoms of positively and negatively charged polar residues are orientationally ordered. This is in agreement with data obtained by other simulations of fully hydrated proteins.[12,14]

The electrostatic properties of the aa residues play an important role in the distribution of the protein−water H-bonds at the protein surface. Most of the water molecules are hydrogen bonded to positively and negatively polar residues as an acceptor or donor of hydrogen atom, respectively. A similar behavior has been reported in the molecular dynamics simulation of copper plastocyanin.[9]

Our investigation provides a detailed picture of the water structure at the protein surface. Water density oscillations near the protein surface due to packing effects are observed. We calculated that the average water density of the first hydration shell of SNase is ∼0.3−0.6% larger than that of the bulk solvent. This tendency is in qualitative agreement with recently reported[73] data obtained by using small-angle X-ray and neutron scattering techniques. Our calculation of the density increase is lower than that predicted from molecular dynamics simulations of fully hydrated lysozyme.[18] They revealed that the first hydration layer is 15% denser than bulk water, but about two-thirds of that value are due to geometrical effects caused by the definition of the protein surface, and only a 5% density increase originates from the perturbation of the average water structure from the bulk. Levitt and Sharon[71] calculated the density of the water at the surface of BPTI using Voronoi polyhedra. A small increase in density for water molecules ∼2.5 Å from the protein atoms and a small decrease in density for water 3−4.5 Å from the surface were observed. We note that an increase or decrease of the density of water in the first hydration shell of the protein depends on the chemical characteristics of the protein surface and that the calculation of the density of the hydration layer is very sensitive to the definition of the volume corresponding to protein and hydrating water, respectively. The broad maximum of the average number of water−water H-bonds in the range 4−6 Å must be due to an increase of the average coordination number of water molecules, which is a consequence of the increased water density in the neighboring coordination shells.

In this work we analyzed the TIP3P H-bond network also in terms of rings of hydrogen-bonded water molecules. A similar analysis was performed for bulk ST2 water (under ambient conditions,[19,21] for supercooled and stretched water[23]), for the ST4 water model (for solutions of methane[33]), for SPC water (solution of hydrophobic and hydrophilic amino acids[34,35]), and for the TIP4P water model (bulk[22] and confined water[28,29]). In particular, we determined the distribution of water-rings in the different hydration layers of our protein. Due to the density oscillation of the water near the protein and due to protein−water H-bond formation, we observe a preferential orientation of the water rings near the protein surface (essentially parallel near nonpolar atoms and perpendicular near polar atoms) when approaching the protein surface. We found that in the first hydration shell of SNase there exist water rings that are located in the hydration shell of side chain carbon atoms and bonded to polar side chain and/or backbone atoms by one or two hydrogen bonds. Also, we observed class I water rings, i.e.,

water rings near a polar atom at the protein surface, at distances 4−6 Å from the protein that are bonded to oxygen or nitrogen atoms by hydrogen bonds and oriented essentially perpendicular to the protein surface. Interestingly, interfacial water structures in a solution of Phe(amide)$_2$, which exhibits a large hydrophobicity, were investigated by the energy minimization method,[74] and the authors found 4-, 5-, and 6-membered cyclic water structures and showed that 6-membered cyclic structures of water are predominant and mainly distributed at the outside of the first hydration shell. Our findings are similar to these data.

To our knowledge, so far no analysis has been reported on the structural properties of water in terms of rings of hydrogen-bonded water molecules for a protein−water system. In fact, the analysis of non-short-circuited water rings provides additional information on the local order of water molecules at the protein surface, and in general, their distribution may serve as a valuable order parameter for describing structural properties of water at biomolecular interfaces. We found that the distribution of water rings sensitively depends on the nature of the nearest protein atom. We note that nearby carbon atoms of the protein invoke a distribution of water rings similar to that shown in simulations of water in spherical pores with slightly hydrophilic substrates.[28] The pronounced pentagon−pentagon and the pentagon−hexagon radial distribution functions for the water rings at the protein surface as well as the increased number of class II rings in the first hydration shell indicate a type of water molecules arrangement that is similar to the structure of clathrate-like cages that are formed around apolar solute molecules in water.[30,75] Interestingly, also a strengthening of water−pore interactions and a decreasing pore size of water confined in porous systems has been shown to increase the clathrate-like character of the water structure in the first hydration layer.[29] The existence of relatively small (4-, 5-, and 6-rings) and large (7-, 8-, and 9-rings) water rings at the protein surface might have the same physical origin as the existence of polygons and hydrogen-bonded chains observed in the first outer layer in hydrophilic pores.[76] As revealed by the organization of water rings around the various protein atoms, we note that both hydration of the hydrophobic protein atoms (clathrate-like arrangement of the water molecules) and interaction with hydrophilic atoms (protein−water hydrogen bonding) are important features of the native, folded protein's surface. A rather complex hydration scenario of the protein surface is observed, which strongly depends on the local surface topography and contains competing contributions of both types of hydrating water molecules.

To conclude, our molecular dynamics simulation run on fully hydrated SNase and the detailed analysis of the structural properties of water indicate that the structural behavior of the water and H-bond network at the protein surface is very complex and depends on the chemical and topographical properties of the protein surface. We note that despite (i) the structural nonuniformity of the protein surface, (ii) the presence of different types of atoms (polar and nonpolar) on the protein surface, and (iii) strong protein−water interactions by hydrogen-bond formation, the general behavior of the population of water rings and the water density oscillation is very similar to that known for smooth surfaces.[28,76] We suppose that the H-bond network structure near the protein surface is not only relevant for the structure and dynamics but also for the biological function of the biomolecule. Hence, we think it is important to study such H-bond networks in terms of their primary units, such as water rings. Such analysis can also be helpful to study the perturbation of the water structure near protein surfaces, for example, in the case of cold denaturation and upon addition of chaotropic and kosmotropic cosolvents. These studies are currently underway. In fact, in experimental studies[77−81] on hydrated lysozyme powders it was reported that the properties of the H-bond network is very important for the enzymatic activity of lysozyme and for the dynamics of protons along chains of hydrogen-bonded water molecules adsorbed on the surface of the protein. These results demonstrate the importance of detailed investigations of the H-bond network at protein surfaces such as that shown in this study.

Acknowledgment. This study was conducted within the Forschergruppe FOR 436 ("Polymorphism, Dynamics and Function of Water at Molecular Interfaces") of the Deutsche Forschungsgemeinschaft (DFG). Financial support by the DFG is gratefully acknowledged. The authors acknowledge various helpful discussions with Drs. Ivan Brovchenko and Alfons Geiger.

References and Notes

(1) Bizzarri, A. R.; Cannistraro, S. *J. Phys. Chem. B* **2002**, *106*, 6617−6633.
(2) Phillips, G. N., Jr.; Pettitt, B. M. *Protein Sci.* **1995**, *4*, 149−158.
(3) Ahlström, P.; Teleman, O.; Jönsson, B. *J. Am. Chem. Soc.* **1988**, *110*, 4198−4203.
(4) Brooks, C. L., III; Karplus, M. *J. Mol. Biol.* **1989**, *208*, 159−181.
(5) Tirado-Rives, J.; Jorgensen, W. L. *J. Am. Chem. Soc.* **1990**, *112*, 2773−2781.
(6) Brunne, R. M.; Liepinsh, E.; Otting, G.; Wüthrich, K.; van Gunsteren, W. F. *J. Mol. Biol.* **1993**, *231*, 1040−1048.
(7) Garcia, A. E.; Stiller, L. *J. Comput. Chem.* **1993**, *14*, 1396−1406.
(8) Lounnas, V.; Pettitt, B. M.; Phillips, G. N., Jr. *Biophys. J.* **1994**, *66*, 601−614.
(9) Bizzarri, A. R.; Wang, C. X.; Chen, W. Z.; Cannistraro, S. *Chem. Phys.* **1995**, *201*, 463−472.
(10) Rocchi, C.; Bizzarri, A. R.; Cannistraro, S. *Phys. Rev. E* **1998**, *57*, 3315−3325.
(11) Makarov, V. A.; Feig, M.; Andrews, B. K.; Pettitt, B. M. *Biophys. J.* **1998**, *75*, 150−158.
(12) Garcia, A. E.; Hummer, G. *Proteins: Struct., Funct., Genet.* **1999**, *36*, 175−191.
(13) Garcia, A. E.; Hummer, G. *Proteins: Struct., Funct., Genet.* **2000**, *38*, 261−272.
(14) Luise, A.; Falconi, M.; Desideri, A. *Proteins: Struct., Funct., Genet.* **2000**, *39*, 56−67.
(15) Makarov, V. A.; Andrews, B. K.; Smith, P. E.; Pettitt, B. M. *Biophy. J.* **2000**, *79*, 2966−2974.
(16) Sterpone, F.; Ceccarelli, M.; Marchi, M. *J. Mol. Biol.* **2001**, *311*, 409−419.
(17) Marchi, M.; Sterpone, F.; Ceccarelli, M. *J. Am. Chem. Soc.* **2002**, *124*, 6787−6791.
(18) Merzel, F.; Smith, J. C. *Proc. Natl. Acad. Sci. U.S.A.* **2002**, *99*, 5378−5383.
(19) Rahman, A.; Stillinger, F. H. *J. Am. Chem. Soc.* **1973**, *95*, 7943−7948.
(20) Speedy, R. J. *J. Phys. Chem.* **1984**, *88*, 3364−3373.
(21) Speedy, R. J.; Mezei, M. *J. Phys. Chem.* **1985**, *89*, 171−175.
(22) Speedy, R. J.; Madura, J. D.; Jorgensen, W. L. *J. Phys. Chem.* **1987**, *91*, 909−913.
(23) Mausbach, P.; Schnitker, J.; Geiger, A. *J. Technol. Phys.* **1987**, *28*, 67−76.
(24) Lee, C. Y.; McCammon, J. A.; Rossky, P. J. *J. Chem. Phys.* **1984**, *80*, 4448−4455.
(25) Lee, C. Y.; Rossky, P. J. *J. Chem. Phys.* **1994**, *100*, 3334−3345.
(26) Werder, T.; Walther, J. H.; Jaffe, R. L.; Halicioglu, T.; Koumoutsakos, P. *J. Phys. Chem. B* **2003**, *107*, 1345−1352.
(27) Brovchenko, I.; Paschek, D.; Geiger, A. *J. Chem. Phys.* **2000**, *113*, 5026−5036.
(28) Brovchenko, I. V.; Geiger, A.; Paschek, D. *Fluid Phase Equilibria* **2001**, *183−184*, 331−339.
(29) Brovchenko, I. V.; Geiger, A. *J. Mol. Liq.* **2002**, *96−97*, 195−206.
(30) Geiger, A.; Rahman, A.; Stillinger, F. H. *J. Chem. Phys.* **1979**, *70*, 263−276.
(31) Zichi, D. A.; Rossky, P. J. *J. Chem. Phys.* **1985**, *83*, 797−808.
(32) Cheng, Y.-K.; Sheu, W. S.; Rossky, P. J. *Biophys. J.* **1999**, *76*, 1734−1743.

(33) Head-Gordon, T. *Proc. Natl. Acad. Soc. U.S.A.* **1995**, *92*, 8308−8312.
(34) Pertsemlidis, A.; Saxena, A. M.; Soper, A. K.; Head-Gordon, T.; Glaeser, R. M. *Proc. Natl. Acad. Sci. U.S.A.* **1996**, *93*, 10769−10774.
(35) Head-Gordon, T.; Sorenson, J. M.; Pertsemlidis, A.; Glaeser, R. M. *Biophys. J.* **1997**, *73*, 2106−2115.
(36) Teeter, M. M. *Proc. Natl. Acad. Sci. U.S.A.* **1984**, *81*, 6014−6018.
(37) Nakasako, M. *J. Biol. Phys.* **2002**, *28*, 129−137.
(38) Lipscomb, L. A.; Peek, M. E.; Zhou, F. X.; Bertrand, J. A.; VanDerveer, D.; Williams, L. D. *Biochemistry* **1994**, *33*, 3649−3659.
(39) Chen, H. M.; Markin, V. S.; Tsong, T. Y. *Biochemistry* **1992**, *31*, 1483−1491.
(40) Carra, J. H.; Anderson, E. A.; Privalov, P. L. *Biochemistry* **1994**, *33*, 10842−10850.
(41) Carra, J. H.; Privalov, P. L. *Biochemistry* **1995**, *34*, 2034−2041.
(42) Vidugiris, G. J. A.; Truckses, D. M.; Markley, J. L.; Royer, C. A. *Biochemistry* **1996**, *35*, 3857−3864.
(43) Eftink, M. R.; Ionescu, R.; Ramsay, G. D.; Wong, C.-Y.; Wu, J. Q.; Maki, A. H. *Biochemistry* **1996**, *35*, 8084−8094.
(44) Hinck, A. P.; Truckses, D. M.; Markley, J. L. *Biochemistry* **1996**, *35*, 10328−10338.
(45) Walkenhorst, W. F.; Green, S. M.; Roder, M. *Biochemistry* **1997**, *36*, 5795−5805.
(46) Panick, G.; Malessa, R.; Winter, R.; Rapp, G.; Frye, K. J.; Royer, C. A. *J. Mol. Biol.* **1998**, *275*, 389−402; Panick, G.; Vidugiris, G. J. A.; Malessa, R.; Rapp, G.; Winter, R.; Royer, C. A. *Biochemistry* **1999**, *38*, 4157−4164.
(47) Kataoka, M.; Ferrand, M.; Goupil-Lammy, A. V.; Kamikubo, H.; Yunoki, J.; Oka, T.; Smith, J. C. *Physica B* **1999**, *266*, 20−26.
(48) Ravindra R.; Royer, C.; Winter, R. *Phys. Chem. Chem. Phys.* **2004**, *6*, 1952−1961.
(49) Filfil, R.; Chalikian, T. V. *J. Mol. Biol.* **2000**, *299*, 827−842.
(50) Seemann, H.; Winter, R.; Royer, C. A. *J. Mol. Biol.* **2001**, *307*, 1091−1102.
(51) Bahar, I.; Wallqvist, A.; Covell, D. G.; Jernigan, R. L. *Biochemistry* **1998**, *37*, 1067−1075.
(52) Zhou, H.-X. *Biophys. J.* **2002**, *83*, 2981−2986.
(53) Yamaotsu, N.; Moriguchi, I.; Kollman, P. A.; Hirono, S. *Biochim. Biophys. Acta* **1993**, *1163*, 81−88.
(54) Lamy, A.; Smith, J. C. *J. Am. Chem. Soc.* **1996**, *118*, 7326−7328.
(55) Ikura, T.; Tsurupa, G. P.; Kuwajima, K. *Biochemistry* **1997**, *36*, 6529−6538.
(56) Chatfield, D. C.; Szabo, A.; Brooks, B. R. *J. Am. Chem. Soc.* **1998**, *120*, 5301−5311.
(57) Wrabl, J. O.; Shortle, D.; Woolf, T. B. *Proteins: Struct., Funct., Genet.* **2000**, *38*, 123−133.
(58) Bernstein, F. C.; Koetzle, T. F.; Williams, G. J. B.; Meyer, E. F., Jr.; Tasumi, M. *J. Mol. Biol.* **1977**, *12*, 535−542. (b) Berman, H. M.; Westbrook, J.; Feng, Z.; Gilliland, G.; Bhat, T. N.; Weissig, H.; Shindyalov, I. N.; Bourne, P. E. *Nucleic Acids Res.* **2000**, *28*, 235−242.
(59) Hynes, T. R.; Fox, R. O. *Proteins: Struct., Funct., Genet.* **1991**, *10*, 92−105.
(60) Case, D. A.; Pearlman, D. A.; Caldwell, J. W.; Cheatham, T. E., III; Ross, W. S.; Simmerling, C. L.; Darden, T. A.; Merz, K. M.; Stanton, R. V.; Cheng, A. L.; Vincent, J. J.; Crowley, M.; Tsui, V.; Radmer, R. J.; Duan, Y.; Pitera, J.; Massova, I.; Seibel, G. L.; Singh, U. C.; Weiner, P. K.; Kollman, P. A. *Amber*, version 6; University of California: San Francisco, CA, 1999.
(61) Cornell, W. D.; Cieplak, P.; Bayly, C. I.; Gould, I. R.; Merz, K. M., Jr.; Ferguson, D. M.; Spellmeyer, D. C.; Fox, T.; Caldwell, J. W.; Kollman, P. A. *J. Am. Chem. Soc.* **1995**, *117*, 5179−5197.
(62) Essmann, U.; Perera, L.; Berkowitz, M. L.; Darden, T.; Lee, H.; Pedersen, L. G. *J. Chem. Phys.* **1995**, *103*, 8577−8593.
(63) Jorgensen, W. L.; Chandrasekhar, J., Madura, J. D.; Impey, R. W.; Klein, M. L. *J. Chem. Phys.* **1983**, *79*, 926−935.
(64) Berendsen, H. J. C.; Postma, J. P. M.; van Gunsteren, W. F.; DiNola, A.; Haak, J. R. *J. Chem. Phys*. **1984**, *81*, 3684−3690.
(65) Ryckaert, J.-P.; Ciccotti, G.; Berendsen, H. J. C. *J. Comput. Chem.* **1977**, *23*, 327−341.
(66) Kabsch, W.; Sander, C. *Biopolymers* **1983**, *22*, 2577−2637.
(67) Mol_Volume is a program in the MDTools utility package at the Theoretical Biophysics group, an NIH Resource for Macromolecular Modeling and Bioinformatics; see http://www.ks.uiuc.edu/Development/MDTools
(68) Humphrey, W.; Dalke, A.; Schulten, K. *J. Mol. Graphics* **1996**, *14.1*, 33−38.
(69) Eisenberg, D.; Kauzmann, W. *The Structure and Properties of Water*; Oxford University Press: New York, 1969.
(70) Richards, F. *Annu. Rev. Biophys. Bioeng.* **1977**, *6*, 151−176.
(71) Svergun, D. I.; Richard, S.; Koch, M. H. J.; Sayers, Z.; Kuprin, S.; Zaccai, G. *Proc. Natl. Acad. Sci. U.S.A.* **1998**, *95*, 2267−2272.
(72) Levitt, M.; Sharon, R. *Proc. Natl. Acad. Sci. U.S.A.* **1988**, *85*, 7557−7561.
(73) Connolly, M. L. *J. Am. Chem. Soc.* **1985**, *107*, 1118−1124.
(74) Kim, S.; Yoon, C. N.; Jhon, M. S. *J. Comput. Chem.* **1988**, *9*, 125−132.
(75) Guillot, B.; Guissani, Y. *J. Chem. Phys.* **1993**, *99*, 8075−8094.
(76) Brovchenko, I.; Geiger, A.; Oleinikova, A. In *New Kinds of Phase Transitons: Transformations in Disordered Substances*; Kluwer Academic Publishers: Norwell, MA, 2002; pp 367−378.
(77) Careri, G.; Giansanti, A.; Rupley, J. A. *Proc. Natl. Acad. Sci. U.S.A.* **1986**, *83*, 6810−6814.
(78) Careri, G.; Giansanti, A.; Rupley, J. A. *Phys. Rev. E* **1988**, *37*, 2703−2705.
(79) Careri, G.; Giansanti, A.; Bruni, F. *Solid State Ionics* **1999**, *125*, 257−261.
(80) Levstik, A.; Filipic, C.; Kutnjak, Z.; Careri, G.; Consolini, G.; Bruni, F. *Phys. Rev. E* **1999**, *60*, 7604−7607.
(81) Pizzitutti, F.; Bruni, F. *Phys. Rev. E* **2001**, *64*, 052905.